Shell correction dependence of potential depth in an α-decay cluster model

Junlong Tian,[1,2] Kai Ren,[1] Pengfei Ma,[1] Cheng Li,[1,2,*] and Ning Wang[1,2,†]
[1]*Department of Physics, Guangxi Normal University, Guilin 541004, People's Republic of China*
[2]*Guangxi Key Laboratory of Nuclear Physics and Technology, Guilin 541004, People's Republic of China*

(Received 25 July 2024; revised 25 October 2024; accepted 27 November 2024; published 13 December 2024; corrected 26 December 2024)

The depth of nuclear potential for α decay is systematically investigated using 178 measured α-decay half-lives of even-even nuclei. We find that, by considering the shell effect in the depth of the potential, the results can be significantly improved. The root-mean-square deviation across the 178 data points is reduced from 0.278 to 0.188 by introducing a new formula that accounts for the shell correction dependence of potential depth. The α-decay half-lives for unknown nuclei with charge numbers $Z = 118$ and 120 are predicted with the proposed formula.

DOI: 10.1103/PhysRevC.110.064313

I. INTRODUCTION

α decay is a primary mode of radioactive decay for heavy nuclei, providing valuable insights into nuclear structures. It plays a crucial role in the experimental identification of new nuclides and elements, especially for heavy and superheavy nuclei. Since the discovery of α decay, numerous physicists have worked to explain this phenomenon. The pioneering law that established a correlation between half-lives and Q values for the systematic study of α decay was formulated by Geiger and Nuttall [1]. They observed that plotting $\log_{10} T_{1/2}$ against $1/\sqrt{Q}$ empirically yields a linear relationship for isotopes. Here, Q represents the total energy released in α decay. The phenomenon of α decay was explained by Gamow [2] and independently by Gurney and Condon [3] as a quantum tunneling process, which is the first application of quantum mechanics in subatomic systems. Since then, various new theoretical models [4–14] were proposed to better understand α decay, but the legacy of the Gamow model remains evident.

The systematics of α decay changes abruptly around neutron closure $N = 126$, showing distinct linear relationships in Geiger-Nuttall plots for $N < 126$ and $N > 126$. This behavior reflects the shell structure effects on half-life, as confirmed by various studies [15–17]. Buck, Merchant, and Perez (BMP) proposed a simple square-well cluster model, known as the BMP model. This model posits that the decay nucleus consists of an "α-core" system with the α particle moving in two distinct orbits around the core. The BMP model effectively reproduces experimental α-decay half-lives for even-even nuclei in the heavy mass region using only three fixed parameters: the global quantum number (G), the α-particle preformation probability (P_α), and the potential depth (V_N). The discontinuity in Geiger-Nuttall plots at $N = 126$ is interpreted as the α cluster occupying different orbits with $G = 22$ for $N < 126$ or 24 for $N > 126$.

In the BMP model, different α emitters are assumed to have the same potential depth, $V_N = 134$ MeV [16], which is a rough approximation of the actual effective potential. Theoretical studies have indicated that the potential depth can provide valuable information about nuclear structure and usually varies between different nuclei [18,19]. Even across different methods, the potential depth varies significantly, ranging from 100 MeV [20] to 1100 MeV [21]. In Ref. [22], an improved square-well cluster model is proposed by taking into consideration that the potential depth (V_N) depends on the mass number (A) and the charge number (Z) of the parent nucleus. In this model, more theoretical data points align with experimental data within a factor of 1.5, compared to a factor of 2 in the BMP model. On the other hand, the shell effect is indispensable for the theoretical model or empirical formulas to accurately reproduce the systematics of α-decay half-lives. Although the α-decay half-life is primarily determined by the Q value, and a main part of the strong shell effect is already included in the Q value, we found that shell effects are still not considered enough (see Fig. 1), especially near the magic number $N = 126$. This issue persists even with different quantum numbers G used in the BMP model according to the Wildermuth condition [16,17]. In Ref. [23], the shell correction is considered for an accurate description of α decay within the generalized liquid drop model, and the shell correction remarkably reduces the deviation between theoretical and experimental half-lives of α decay around the neutron shell closure $N = 126$. Therefore, it is crucial to further consider the nuclear shell structure effect.

Inspired by Refs. [22,23], in order to address the aforementioned problems, it is intriguing to establish a correlation between the potential depth V_N and the shell correction energy $E_{\rm sh}$ of the α emitter. In this work, we attempt to propose a new formula for potential depth by fitting the extracted "experimental" values, considering the shell correction within the BMP model. This approach is referred to as the improved BMP (ImBMP) model.

*Contact author: licheng@mail.bnu.edu.cn
†Contact author: wangning@gxnu.edu.cn

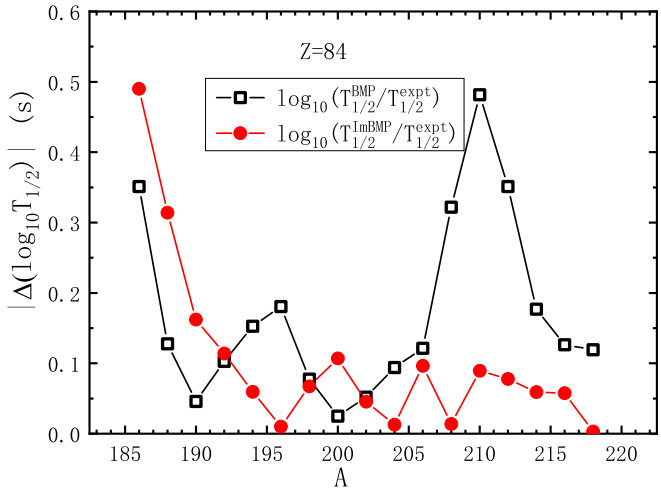

FIG. 1. Absolute value of logarithms of the ratios between theoretical α-decay half-lives and experimental ones for the even-even Po isotopic chain with the BMP model (open squares) and with Eq. (12) (solid circles) for V_N in the ImBMP model.

II. THEORETICAL FRAMEWORK

A. Buck-Merchant-Perez (BMP) model

The nuclear potential for an α particle inside a nucleus is a key concept for investigating α-decay half-lives of nuclei in the cluster model. Buck *et al.* employed various potential forms—including a square-well [16], a cosh [24], and a mixed Woods-Saxon potential [25]—and achieved similar results in evaluating measured α-decay half-lives. However, the square-well potential is the simplest approach. Since our focus is on exploring the effects of nuclear shell corrections on the nuclear potential, we use the square-well potential for the α particle due to its simplicity. The square-well potential assumes that nuclei have well-defined boundaries, as postulated in the liquid drop model. By assuming a uniform density, the α-core effective potential $V(r)$ is defined as the sum of the Coulomb potential and the nuclear square-well potential,

$$V(r) = \begin{cases} -V_0 = -V_N + \frac{C}{R} & (r < R), \\ C/r & (r > R), \end{cases} \tag{1}$$

where the product of charges $C = Z_\alpha Z_d e^2$, and Z_α and Z_d are the proton numbers of the α particle and the daughter nucleus, respectively. In the Gamow model, the potential $V(r) = -V_0$ is constant. In contrast, the BMP model allows the potential to vary by including the surface Coulomb potential. This leads to more accurate results in the BMP model than in the Gamow model. The radius R and the depth V_N of square-well potential are related by the Bohr-Sommerfeld quantization condition. For an $L = 0$ α particle with global quantum number G and a corresponding Q value, the result is

$$\int_0^R \sqrt{\frac{2\mu}{\hbar^2}[Q - V(r)]}dr = \frac{\pi}{2}(G+1), \tag{2}$$

where $\mu = A_\alpha A_d \mathrm{u}/(A_\alpha + A_d)$ is the reduced mass of the α-daughter system, and A_α and A_d are the atomic mass numbers of α particle and the daughter nucleus, respectively. Here, $\mathrm{u} = 931.494\ \mathrm{MeV/c^2}$ is the atomic mass unit and $c = 3.0 \times 10^{23}$ fm/s is the speed of light. The experimental Q values used in the present calculations are sourced from the AME2020 mass table [26]. For unmeasured Q values, we use the Weizsäcker–Skyrme 4 (WS4) mass table [27]. Many references [14,28,29] confirm the accuracy of the WS4 mass model in reproducing the experimental Q values for various decay modes.

The square-well radius R is determined by solving the system formed by combining Eqs. (1) and (2) as follows:

$$R = \frac{C + \sqrt{C^2 + 4(Q+V_N)\frac{\hbar^2}{2\mu}\left[\frac{\pi}{2}(G+1)\right]^2}}{2(Q+V_N)}. \tag{3}$$

The radius R is a crucial ingredient in the expression for the decay width Γ, which is given in the semiclassical approximation [30] by

$$\Gamma = \frac{P_\alpha \hbar^2 K}{2\mu R}\exp\left[-2\int_R^{C/Q} k(r)dr\right]. \tag{4}$$

Here, P_α represents the α-particle preformation probability, while K and $k(r)$ are the wave numbers in the internal and barrier regions, respectively,

$$K = \left[\frac{2\mu}{\hbar^2}\left(Q + V_N - \frac{C}{R}\right)\right]^{1/2}, \tag{5}$$

$$k(r) = \left[\frac{2\mu}{\hbar^2}\left(\frac{C}{r} - Q\right)\right]^{1/2}. \tag{6}$$

The relationship between the half-life and decay width in α decay is given by

$$T_{1/2} = \frac{\hbar \ln 2}{\Gamma} = \frac{2\mu R \ln 2}{\hbar K P_\alpha}\exp\left[2\int_R^{C/Q} k(r)dr\right]. \tag{7}$$

Given the integral conditions $Q > 0$ and $\frac{C}{Q} > R > 0$ in Eq. (7), the action integral can be analytically derived as follows:

$$2\int_R^{C/Q} k(r)dr = 2\sqrt{\frac{2\mu}{\hbar^2}}\frac{C}{\sqrt{Q}} \times \left[\arccos\left(\sqrt{\frac{QR}{C}}\right) - \sqrt{\frac{QR}{C} - \left(\frac{QR}{C}\right)^2}\right]. \tag{8}$$

By inserting the action integral Eq. (8) into Eq. (7) and taking the decimal logarithm, we can analytically obtain decay formula in accordance with the form of the Geiger-Nuttall Law as in Ref. [31],

$$\log_{10} T_{1/2} = a + bQ^{-1/2}, \tag{9}$$

where a and b are decay parameters as follows:

$$a = \log_{10}\left(\frac{4\mu R^2 \ln 2}{P_\alpha \pi \hbar (G+1)}\right), \tag{10}$$

$$b = 2\sqrt{\frac{2\mu}{\hbar^2}C\log_{10}(e)} \times \left[\arccos\left(\sqrt{\frac{QR}{C}}\right) - \sqrt{\frac{QR}{C} - \left(\frac{QR}{C}\right)^2}\right]. \tag{11}$$

B. Shell correction dependence of potential depth

Figure 1 presents the absolute value of $\Delta(\log_{10}T_{1/2})$ for the even-even Po isotopic chain. The open squares represent the BMP model results with $V_N = 134$ MeV, while the solid circles correspond to the ImBMP model results, calculated using Eq. (12). Here, $\Delta(\log_{10} T_{1/2}) = \log_{10}(T^{\rm cal}_{1/2}/T^{\rm expt}_{1/2})$ represents the logarithms of the ratios between theoretical and experimental α-decay half-lives. As shown in Fig. 1, a dramatic deviation in $\Delta(\log_{10} T_{1/2})$ occurs around the magic number $N = 126$ on the even-even Po isotopic chain using the BMP model. In contrast, values calculated using Eq. (12) show much better agreement with the experimental data at $N = 126$. This trend is also observed for other isotopic chains across the neutron magic number 126. The systematic variation seems linked to the corresponding shell structures, which implies that considering the potential depth including shell correction could be helpful for a better description of the half-lives of α decay.

In this work, our goal is to propose a straightforward formula for the potential depth V_N, that depends on the properties of the individual α emitter based on the BMP model. First, the "experimental" potential depth $V_N^{\rm expt}$ can be extracted using Eq. (3) along with Eqs. (9)–(11), based on the measured half-life of $T_{1/2}^{\rm expt}$ by the enumeration method. This calculation assumes a constant α-particle preformation probability $P_\alpha = 1$, as used in the BMP model. For this analysis, 178 measured half-lives of even-even nuclei with atomic numbers Z ranging from 60 to 118 were utilized. These nuclei were selected based on an error margin within 30% from the data listed for even-even nuclei in the NUBASE2020 database [32]. Detailed information on the potential depths and widths, shell correction energies, Q values, and both theoretical and experimental half-lives of α decay for 178 even-even nuclei are listed in Table I. These data help determine the potential depths characterizing α-core interactions within parent nuclei. We demonstrate that this potential depth can reliably predict the α-decay half-lives of unmeasured nuclei. To construct the V_N formula, we begin by plotting the experimental depth $V_N^{\rm expt}$ against the mass number A of parent nuclei, as shown in Fig. 2. The open squares represent the extracted potential depths $V_N^{\rm expt}$ (listed in column 4 of Table I) derived from the measured α-decay half-lives of 178 even-even nuclei. The average value of the open squares is approximately 134 MeV, marked by a dashed line, which matches the value used in the BMP model [16]. Figure 2 shows that the experimental potential depth $V_N^{\rm expt}$ is not constant but varies depending on the structure of different α emitters. For the open squares,

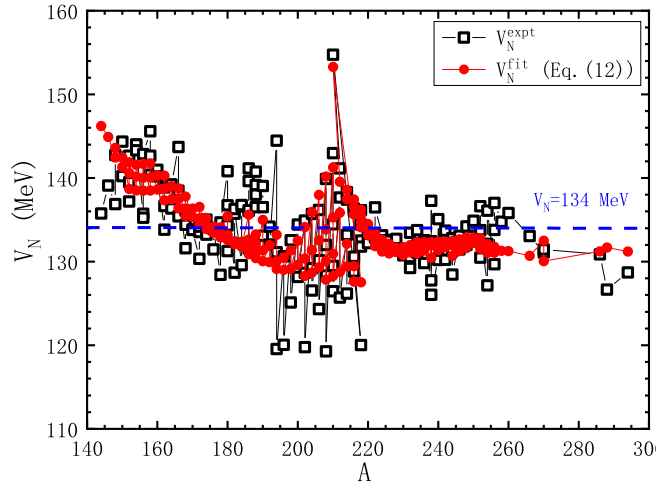

FIG. 2. Values of V_N as a function of mass numbers of parent nuclei. The open squares denote the extracted potential depths $V_N^{\rm expt}$ from the measured α-decay half-lives of 178 even-even nuclei. The solid circles denote the calculation results with Eq. (12). The average value of the open squares equals approximately to 134 MeV marked with a dashed line.

$V_N^{\rm expt}$ initially tends to decrease, exhibiting fluctuations with increasing mass number. However, it increases abruptly at the $N = 126$ shell closure (reaching a maximum value of 154.741 MeV for ^{210}Pb), and then subsequently drops to around 134 MeV, continuing to fluctuate thereafter. It is found that the shell effect plays a crucial role for some nuclei, particularly around the neutron magic number 126. Although we cannot account for the unique properties of each individual nucleus, we can consider the shell correction energy $E_{\rm sh}$ of the parent nucleus. The shell correction energy $E_{\rm sh}$ can be derived from some mass tables or calculated as the difference between experimental and macroscopic binding energies of the nucleus.

Next, we explore various combinations of mass number A, charge number Z, isospin asymmetry $I = (N - Z)/A$, and shell correction $E_{\rm sh}$. Our goal is to develop a new formula for the potential depth V_N, applicable to different α emitters. We propose a new formula for V_N, which relates the potential depth to shell correction energy, based on a fit to the extracted experimental values $V_N^{\rm expt}$ (see Fig. 2). To ensure high-accuracy calculations with minimal parameters, we find that Eq. (12) closely matches the experimental values $V_N^{\rm expt}$ extracted from experimental α-decay half-lives:

$$V_N^{\rm fit} = c_0 + \left(c_1 A^2 + c_2 A + c_3 E_{\rm sh}\frac{AZ}{Q}\right)\Big/ G, \tag{12}$$

where the coefficients $c_0 = 211$ MeV, $c_1 = 0.0203$ MeV, $c_2 = -13.1878$ MeV, and $c_3 = 0.0095$ MeV are obtained from a least-squares fit to the experimental potential depths $V_N^{\rm expt}$ of 178 data points. In Eq. (12), the last term, $E_{\rm sh}AZ/Q$, is a dimensionless quantity that indicates the proportion of shell correction energy relative to the total decay energy for the given nucleus (A, Z). A larger value of this ratio corresponds to a deeper potential well, which may increase the difficulty of penetrating the potential barrier during the α decay

TABLE I. Comparison of the experimental data for α-decay nuclei with calculated results. The Q values are taken from AME2020 [26], the shell correction energies $E_{\rm sh}$ are calculated using Eq. (13), and $V_N^{\rm expt}$ and $V_N^{\rm fit}$ are the extracted "experimental" potential depths and their fitting values. $R^{(1)}$ and $R^{(2)}$ are the calculated radii of square wells with Eq. (3) based on $V_N^{\rm expt}$ and $V_N^{\rm fit}$. The experimental α-decay half-lives $\log_{10} T_{1/2}^{\rm expt}$ are taken from NUBASE2020 [32], and $\log_{10} T_{1/2}^{\rm cal}$ and $\log_{10} T_{1/2}^{\rm BMP}$ are the logarithms of half-lives calculated with and without considering shell corrections, respectively.

α emitter	Q (MeV)	$E_{\rm sh}$ (MeV)	$V_N^{\rm expt}$ (MeV)	$V_N^{\rm fit}$ (MeV)	$R^{(1)}$ (fm)	$R^{(2)}$ (fm)	$\log T_{1/2}^{\rm expt}$ (s)	$\log T_{1/2}^{\rm BMP}$ (s)	$\log T_{1/2}^{\rm cal}$ (s)
^{144}Nd	1.901	1.715	135.765	147.199	7.771	7.442	22.859	22.774	23.372
^{146}Sm	2.529	1.125	139.097	144.919	7.673	7.507	15.332	15.091	15.592
^{148}Sm	1.987	−0.049	136.888	142.437	7.754	7.591	23.298	23.157	23.556
^{148}Gd	3.271	0.857	142.744	143.599	7.567	7.543	9.352	8.947	9.389
^{150}Gd	2.807	−0.403	140.238	141.294	7.651	7.620	13.752	13.455	13.800
^{150}Dy	4.351	0.611	144.361	142.483	7.512	7.564	3.107	2.638	3.024
^{152}Gd	2.204	−1.349	137.205	138.687	7.758	7.713	21.532	21.373	21.602
^{152}Dy	3.727	−0.575	139.489	140.581	7.667	7.635	6.930	6.670	6.979
^{152}Er	4.934	0.710	142.673	141.884	7.563	7.585	1.057	0.660	1.021
^{154}Dy	2.945	−1.418	143.961	138.510	7.560	7.717	13.976	13.501	13.721
^{154}Er	4.280	−0.416	144.007	140.175	7.542	7.651	4.677	4.211	4.503
^{154}Yb	5.474	1.140	143.309	141.577	7.550	7.599	−0.355	−0.782	−0.433
^{156}Er	3.481	−1.141	135.733	138.493	7.806	7.723	9.989	9.902	10.122
^{156}Yb	4.810	0.041	135.249	140.026	7.803	7.661	2.408	2.346	2.633
^{156}Hf	6.026	2.116	142.863	141.680	7.567	7.600	−1.638	−2.047	−1.692
^{158}Hf	4.170	−0.742	145.589	138.523	7.521	7.723	6.6291	6.078	6.300
^{158}W	5.405	0.756	140.380	140.051	7.654	7.663	0.808	0.503	0.792
^{158}Yb	6.613	3.109	142.675	141.729	7.576	7.603	−2.845	−3.247	−2.888
^{160}Hf	4.902	−0.125	140.975	138.631	7.650	7.719	3.276	2.938	3.164
^{160}W	6.066	1.877	140.195	140.331	7.661	7.657	−0.989	−1.285	−0.984
^{162}Hf	4.416	−0.722	133.807	137.334	7.879	7.771	5.687	5.696	5.862
^{162}W	5.678	0.647	136.655	138.740	7.776	7.713	0.420	0.289	0.519
^{162}Os	6.768	2.732	138.888	140.288	7.699	7.658	−2.678	−2.913	−2.614
^{164}W	5.278	−0.107	136.337	137.452	7.796	7.763	2.218	2.101	2.272
^{164}Os	6.479	1.777	139.243	139.026	7.696	7.702	−1.662	−1.916	−1.673
^{166}W	4.856	−0.550	143.699	136.371	7.592	7.807	4.738	4.263	4.383
^{166}Os	6.143	0.638	135.413	137.532	7.819	7.755	−0.593	−0.664	−0.490
^{166}Pt	7.292	2.349	138.488	138.761	7.715	7.707	−3.532	−3.749	−3.520
^{168}W	4.501	−0.801	131.594	135.437	7.967	7.846	6.200	6.325	6.398
^{168}Os	5.816	−0.044	134.399	136.346	7.860	7.800	0.685	0.664	0.781
^{168}Pt	6.990	1.715	136.098	137.768	7.794	7.744	−2.695	−2.799	−2.615
^{170}Os	5.537	−0.488	133.861	135.325	7.884	7.839	1.889	1.895	1.962
^{170}Pt	6.707	0.623	133.791	136.343	7.873	7.794	−1.856	−1.847	−1.730
^{172}Os	5.224	−0.696	130.338	134.499	8.006	7.873	3.207	3.398	3.424
^{172}Pt	6.463	−0.067	133.530	135.188	7.887	7.836	−0.994	−0.971	−0.911
^{172}Hg	7.524	1.666	134.173	136.556	7.857	7.785	−3.636	−3.646	−3.520
^{174}Os	4.871	−0.664	133.580	133.913	7.912	7.901	5.251	5.272	5.267
^{174}Pt	6.183	−0.492	133.218	134.224	7.905	7.874	0.061	0.100	0.111
^{174}Hg	7.233	0.642	135.042	135.219	7.839	7.833	−2.699	−2.752	−2.691
^{176}Pt	5.885	−0.685	131.465	133.450	7.969	7.906	1.197	1.328	1.300
^{176}Hg	6.897	0.051	133.885	134.181	7.884	7.874	−1.651	−1.646	−1.637
^{178}Pt	5.573	−0.642	128.439	132.905	8.078	7.932	2.428	2.724	2.667
^{178}Hg	6.577	−0.316	133.649	133.298	7.900	7.911	−0.526	−0.509	−0.545
^{178}Pb	7.789	0.632	134.692	134.101	7.853	7.871	−3.602	−3.638	−3.633
^{180}W	2.515	1.034	140.820	135.408	7.737	7.903	25.701	25.335	25.413
^{180}Pt	5.276	−0.424	131.260	132.571	7.994	7.952	4.028	4.173	4.097
^{180}Hg	6.259	−0.470	134.318	132.590	7.888	7.943	0.730	0.713	0.639
^{180}Pb	7.419	0.179	136.736	133.208	7.801	7.910	−2.387	−2.526	−2.567
^{182}Pt	4.951	−0.149	128.673	132.343	8.089	7.969	5.623	5.912	5.824
^{182}Hg	5.996	−0.426	135.736	132.082	7.852	7.967	1.892	1.801	1.699
^{182}Pb	7.066	−0.089	136.295	132.445	7.824	7.944	−1.260	−1.379	−1.459
^{184}Pt	4.599	0.285	129.581	132.386	8.070	7.978	7.768	8.010	7.922

TABLE I. (*Continued.*)

α emitter	Q (MeV)	E_{sh} (MeV)	V_N^{expt} (MeV)	V_N^{fit} (MeV)	$R^{(1)}$ (fm)	$R^{(2)}$ (fm)	$\log T_{1/2}^{expt}$ (s)	$\log T_{1/2}^{BMP}$ (s)	$\log T_{1/2}^{cal}$ (s)
^{184}Hg	5.660	−0.171	136.597	131.813	7.835	7.985	3.442	3.305	3.188
^{184}Pb	6.774	−0.202	136.760	131.811	7.818	7.973	−0.213	−0.356	−0.472
^{186}Os	2.821	1.919	136.071	135.619	7.893	7.907	22.800	22.685	22.774
^{186}Pt	4.320	0.802	131.585	132.646	8.012	7.977	9.728	9.860	9.786
^{186}Hg	5.204	0.253	136.142	131.799	7.862	8.000	5.701	5.586	5.466
^{186}Pb	6.471	−0.134	139.626	131.353	7.741	7.996	1.072	0.782	0.640
^{186}Po	8.501	−0.733	141.165	130.910	7.659	7.968	−4.469	−4.820	−4.978
^{188}Pt	4.007	1.455	140.745	133.268	7.736	7.967	12.528	12.169	12.128
^{188}Hg	4.709	0.860	139.156	132.162	7.784	8.003	8.722	8.446	8.344
^{188}Pb	6.109	0.201	138.011	131.199	7.799	8.012	2.468	2.257	2.105
^{188}Po	8.082	−0.680	136.511	130.411	7.807	7.997	−3.569	−3.697	−3.883
^{190}Pt	3.269	2.322	139.053	135.004	7.808	7.934	19.183	18.905	18.961
^{190}Pb	5.698	0.746	136.530	131.358	7.856	8.020	4.245	4.109	3.964
^{190}Po	7.693	−0.482	133.100	130.052	7.923	8.021	−2.611	−2.565	−2.773
^{192}Pb	5.222	1.539	134.180	131.982	7.943	8.014	6.546	6.535	6.423
^{192}Po	7.320	−0.050	132.038	129.941	7.968	8.036	−1.492	−1.389	−1.606
^{194}Pb	4.738	2.565	144.470	133.203	7.647	7.989	9.944	9.386	9.341
^{194}Po	6.987	0.559	131.136	130.063	8.007	8.042	−0.407	−0.254	−0.467
^{194}Rn	7.862	−0.421	119.556	129.120	8.403	8.068	−3.108	−2.297	−2.560
^{196}Po	6.658	1.384	130.659	130.496	8.032	8.038	0.775	0.956	0.765
^{196}Rn	7.617	−0.001	120.067	129.025	8.392	8.078	−2.328	−1.541	−1.811
^{198}Po	6.310	2.469	132.557	131.351	7.981	8.020	2.266	2.344	2.198
^{198}Rn	7.349	0.579	125.104	129.132	8.220	8.083	−1.163	−0.669	−0.935
^{200}Po	5.982	3.662	134.437	132.510	7.931	7.993	3.793	3.768	3.686
^{200}Rn	7.043	1.440	128.172	129.603	8.124	8.077	0.070	0.392	0.150
^{202}Po	5.701	5.070	134.926	134.119	7.924	7.949	5.143	5.091	5.098
^{202}Rn	6.774	2.489	128.643	130.379	8.117	8.059	1.09	1.388	1.187
^{202}Ra	7.880	0.661	119.764	128.277	8.417	8.116	−2.387	−1.572	−1.887
^{204}Po	5.485	6.520	135.689	135.939	7.906	7.898	6.275	6.181	6.288
^{204}Rn	6.547	3.632	129.215	131.369	8.105	8.033	2.012	2.279	2.133
^{204}Ra	7.637	1.477	126.546	128.680	8.182	8.110	−1.222	−0.806	−1.101
^{206}Po	5.327	8.041	136.175	137.968	7.895	7.840	7.144	7.023	7.240
^{206}Rn	6.384	4.875	130.165	132.559	8.078	7.999	2.737	2.951	2.871
^{206}Ra	7.415	2.468	124.331	129.339	8.266	8.094	−0.62	−0.071	−0.330
^{208}Po	5.216	9.622	139.879	140.160	7.784	7.776	7.961	7.639	7.975
^{208}Rn	6.261	6.144	132.006	133.856	8.020	7.961	3.367	3.477	3.469
^{208}Ra	7.273	3.453	128.355	130.048	8.132	8.075	0.104	0.420	0.200
^{208}Th	8.200	1.540	119.260	127.825	8.447	8.142	−2.62	−1.766	−2.110
^{210}Po	5.408	10.982	142.981	141.276	7.687	7.737	7.078	6.596	6.989
^{210}Rn	6.159	7.450	134.471	135.272	7.944	7.919	3.954	3.927	3.997
^{210}Ra	7.151	4.545	129.485	130.934	8.097	8.049	0.602	0.854	0.683
^{210}Th	8.069	2.384	126.457	128.287	8.193	8.130	−1.796	−1.372	−1.691
^{212}Rn	6.385	8.462	137.657	135.849	7.837	7.893	3.157	2.958	3.059
^{212}Th	7.958	3.204	125.711	128.770	8.222	8.117	−1.499	−1.030	−1.322
^{214}Ra	7.273	6.364	133.208	132.138	7.970	8.005	0.387	0.429	0.327
^{214}Th	7.827	4.116	126.178	129.409	8.209	8.100	−1.06	−0.617	−0.874
^{216}Th	8.072	4.654	130.230	129.470	8.064	8.089	−1.58	−1.372	−1.624
^{216}U	8.531	2.948	130.579	127.605	8.061	8.160	−2.161	−1.972	−2.332
^{218}U	8.775	3.342	120.040	127.540	8.419	8.153	−3.451	−2.644	−3.005
^{210}Pb	3.792	11.360	154.741	153.293	7.962	8.002	16.567	15.451	16.494
^{212}Po	8.954	8.882	141.165	139.553	8.225	8.274	−6.531	−6.882	−6.609
^{214}Po	7.834	7.048	137.406	138.588	8.376	8.338	−3.786	−3.963	−3.727
^{214}Rn	9.208	6.681	138.315	137.478	8.326	8.352	−6.587	−6.804	−6.629
^{216}Po	6.906	5.417	136.343	137.455	8.440	8.404	−0.842	−0.969	−0.784
^{216}Rn	8.198	5.260	128.807	136.544	8.674	8.413	−4.538	−4.258	−4.125
^{216}Ra	9.526	4.817	136.037	135.635	8.409	8.422	−6.764	−6.869	−6.785

TABLE I. (*Continued.*)

α emitter	Q (MeV)	$E_{\rm sh}$ (MeV)	$V_N^{\rm expt}$ (MeV)	$V_N^{\rm fit}$ (MeV)	$R^{(1)}$ (fm)	$R^{(2)}$ (fm)	$\log T_{1/2}^{\rm expt}$ (s)	$\log T_{1/2}^{\rm BMP}$ (s)	$\log T_{1/2}^{\rm cal}$ (s)
^{218}Po	6.115	4.015	136.148	136.222	8.471	8.469	2.269	2.150	2.272
^{218}Rn	7.263	4.010	132.529	135.563	8.577	8.475	−1.472	−1.392	−1.307
^{218}Ra	8.540	3.681	131.811	134.743	8.581	8.483	−4.587	−4.470	−4.431
^{218}Th	9.849	3.317	134.450	134.089	8.471	8.483	−6.914	−6.938	−6.934
^{220}Rn	6.405	2.885	132.655	134.487	8.601	8.539	1.745	1.820	1.847
^{220}Ra	7.594	2.874	133.123	134.016	8.568	8.538	−1.742	−1.694	−1.694
^{220}Th	8.973	2.331	132.227	133.156	8.574	8.543	−4.991	−4.896	−4.942
^{222}Rn	5.590	1.933	132.911	133.380	8.620	8.604	5.519	5.581	5.545
^{222}Ra	6.678	2.201	132.907	133.316	8.606	8.592	1.526	1.587	1.548
^{222}Th	8.133	1.745	133.088	132.469	8.573	8.594	−2.65	−2.600	−2.686
^{222}U	9.480	1.263	136.496	131.853	8.438	8.592	−5.328	−5.462	−5.579
^{224}Ra	5.789	1.617	133.156	132.606	8.627	8.646	5.497	5.546	5.464
^{224}Th	7.299	1.430	132.566	131.993	8.618	8.638	0.017	0.098	−0.017
^{224}U	8.628	0.826	131.955	131.215	8.617	8.642	−3.402	−3.289	−3.445
^{226}Ra	4.871	1.259	132.572	132.125	8.679	8.695	10.703	10.789	10.675
^{226}Th	6.453	1.276	131.751	131.685	8.676	8.678	3.265	3.397	3.260
^{226}U	7.701	0.842	132.487	130.997	8.630	8.682	−0.57	−0.484	−0.658
^{228}Th	5.520	1.308	131.383	131.687	8.721	8.710	7.781	7.939	7.799
^{228}U	6.800	1.138	132.734	131.154	8.652	8.707	2.748	2.822	2.652
^{230}Th	4.770	1.345	130.839	131.747	8.767	8.734	12.376	12.572	12.432
^{230}U	5.993	1.462	130.757	131.483	8.749	8.724	6.243	6.441	6.287
^{230}Pu	7.178	1.097	131.328	130.751	8.710	8.731	2.021	2.180	1.985
^{232}Th	4.082	1.409	129.252	131.972	8.850	8.750	17.645	17.949	17.821
^{232}U	5.414	1.746	130.548	131.844	8.777	8.731	9.337	9.551	9.418
^{232}Pu	6.716	1.545	133.446	131.109	8.652	8.734	4.005	4.037	3.862
^{234}U	4.858	2.010	131.070	132.332	8.778	8.733	12.889	13.074	12.969
^{234}Pu	6.310	1.972	131.970	131.531	8.717	8.733	5.723	5.847	5.695
^{234}Cm	7.365	1.776	133.763	130.958	8.641	8.739	2.285	2.298	2.113
^{236}U	4.573	2.042	129.839	132.340	8.833	8.742	14.869	15.135	15.030
^{236}Pu	5.867	2.375	132.558	132.058	8.712	8.729	7.955	8.043	7.923
^{236}Cm	7.067	2.216	132.317	131.320	8.701	8.736	3.351	3.453	3.289
^{238}U	4.270	2.003	127.742	132.272	8.922	8.755	17.149	17.558	17.447
^{238}Pu	5.593	2.611	132.431	132.339	8.725	8.728	9.442	9.539	9.435
^{238}Cm	6.670	2.746	137.263	131.931	8.545	8.728	5.314	5.116	4.988
^{238}Cf	8.130	1.966	126.027	130.448	8.914	8.752	−0.076	0.416	0.201
^{240}Pu	5.256	2.629	130.416	132.381	8.809	8.738	11.316	11.544	11.441
^{240}Cm	6.398	3.127	135.095	132.371	8.627	8.722	6.419	6.351	6.249
^{240}Cf	7.711	2.853	130.199	131.364	8.776	8.734	1.612	1.844	1.683
^{242}Pu	4.984	2.546	130.226	132.232	8.826	8.753	13.073	13.315	13.202
^{242}Cm	6.216	3.209	132.745	132.379	8.714	8.727	7.148	7.225	7.124
^{242}Cf	7.517	3.289	133.710	131.742	8.658	8.727	2.534	2.551	2.412
^{244}Pu	4.666	2.461	131.254	132.144	8.799	8.767	15.41	15.587	15.467
^{244}Cm	5.902	3.257	132.807	132.471	8.723	8.735	8.757	8.831	8.735
^{244}Cf	7.329	3.541	132.786	131.930	8.697	8.727	3.190	3.264	3.136
^{244}Fm	8.550	2.966	128.447	130.714	8.831	8.750	−0.506	−0.166	−0.366
^{246}Cm	5.475	3.273	132.873	132.670	8.735	8.742	11.172	11.243	11.158
^{246}Cf	6.862	3.801	133.097	132.371	8.701	8.727	5.109	5.164	5.063
^{246}Fm	8.379	3.590	131.474	131.262	8.728	8.736	0.218	0.371	0.204
^{248}Cm	5.162	3.159	131.998	132.588	8.777	8.756	13.079	13.208	13.116
^{248}Cf	6.361	4.024	134.204	132.904	8.680	8.725	7.460	7.446	7.377
^{248}Fm	7.995	3.923	132.312	131.643	8.712	8.736	1.538	1.641	1.495
^{250}Cf	6.129	3.986	134.181	132.869	8.688	8.734	8.616	8.604	8.532
^{250}Fm	7.557	4.335	134.888	132.243	8.637	8.729	3.270	3.214	3.105
^{252}Cf	6.217	3.459	130.473	131.758	8.817	8.770	7.935	8.161	8.017
^{252}Fm	7.154	4.655	136.627	132.804	8.591	8.723	4.961	4.798	4.723
^{252}No	8.549	4.374	133.755	131.526	8.665	8.742	0.562	0.576	0.423

TABLE I. (*Continued.*)

α emitter	Q (MeV)	$E_{\rm sh}$ (MeV)	$V_N^{\rm expt}$ (MeV)	$V_N^{\rm fit}$ (MeV)	$R^{(1)}$ (fm)	$R^{(2)}$ (fm)	$\log T_{1/2}^{\rm expt}$ (s)	$\log T_{1/2}^{\rm BMP}$ (s)	$\log T_{1/2}^{\rm cal}$ (s)
^{254}Cf	5.927	2.996	127.172	131.060	8.950	8.805	9.224	9.672	9.482
^{254}Fm	7.307	4.147	132.123	131.783	8.741	8.753	4.067	4.184	4.044
^{254}No	8.226	4.809	136.094	132.070	8.595	8.734	1.755	1.626	1.506
^{256}Fm	7.025	3.618	129.680	131.063	8.839	8.789	5.064	5.339	5.153
^{256}No	8.582	4.478	133.802	131.236	8.661	8.751	0.466	0.477	0.307
^{256}Rf	8.926	5.029	137.012	131.778	8.563	8.742	0.327	0.144	0.006
^{258}Rf	9.196	4.912	134.787	131.287	8.629	8.750	−0.595	−0.644	−0.811
^{260}Sg	9.901	5.331	135.815	131.266	8.592	8.748	−1.772	−1.882	−2.050
^{266}Hs	10.346	5.394	133.058	130.698	8.692	8.775	−2.409	−2.352	−2.556
^{270}Hs	9.070	6.391	131.088	132.510	8.805	8.755	0.954	1.139	1.045
^{270}Ds	11.117	5.365	131.453	130.063	8.743	8.792	−3.688	−3.533	−3.775
^{286}Fl	10.360	6.502	130.871	131.224	8.834	8.821	−0.658	−0.456	−0.636
^{288}Fl	10.076	6.731	126.671	131.677	8.999	8.815	−0.185	0.303	0.151
^{294}Og	11.870	7.380	128.698	131.197	8.904	8.814	−3.155	−2.812	−2.992

process, thereby making the nucleus more stable. Conversely, a smaller ratio implies a shallower potential well, increasing the likelihood of the nucleus undergoing decay. The quantum numbers $G = 22$ for $N < 126$ and $G = 24$ for $N > 126$ are adopted, consistent with G values used in Ref. [16]. The shell correction energy $E_{\rm sh}$ (which includes the pairing term and other residual interaction terms) for the parent nucleus is listed in column 3 of Table I. It is estimated by the difference between the experimental binding energy $B_{\rm expt}$ and the macroscopic binding energy B_m of the nucleus,

$$E_{\rm sh}(A,Z) = B_{\rm expt}(A,Z) - B_{\rm m}(A,Z). \tag{13}$$

The smooth liquid-drop energy of a spherical nucleus B_m is described by a modified Bethe-Weizsäcker mass formula [27],

$$B_m(A,Z) = a_v A - a_s A^{2/3} - a_c \frac{Z^2}{A^{1/3}}(1 - 0.76Z^{-2/3}) - a_{\rm sym} I^2 A f_s, \tag{14}$$

where the symmetry energy coefficient of nuclei is expressed as $a_{\rm sym} = c_{\rm sym}(1 - \frac{\kappa}{A^{1/3}} + \xi\frac{2-|I|}{2+|I|})$ and the correction factor for the symmetry energy is expressed as $f_s = 1 + \kappa_s \epsilon A^{1/3}$ due to the surface diffuseness. Here, $\epsilon = (I - I_0)^2 - I^4$ denotes the correction factor to the constant surface diffuseness of the Woods–Saxon potential and $I_0 = 0.4A/(A + 200)$ denotes the isospin asymmetry of the nuclei along the β-stability line described by Green's formula. Here the coefficients are $a_v = 15.5181$ MeV, $a_s = 17.4090$ MeV, $a_c = 0.7092$ MeV, $c_{\rm sym} = 30.1594$ MeV, $\kappa = 1.5189$, $\xi = 1.2230$, and $\kappa_s = 0.1536$. Figure 2 presents a comparison between the extracted experimental potential depths $V_N^{\rm expt}$ (open squares) and the calculated values $V_N^{\rm fit}$ (solid circles) using Eq. (12). The Pearson correlation coefficient for this comparison is $r = 0.75$. In addition, the calculated half-lives using Eq. (12) are compared with the results of the BMP model with $V_N = 134$ MeV. We found that this approach significantly reduces the root-mean-square (rms) deviation between theoretical and experimental α-decay half-lives from 0.278 to 0.188, resulting in a 32% improvement. The rms deviation is calculated as $\text{rms} = \sqrt{\sum_{i=1}^{178}[\log_{10}(T_{1/2}^{\text{expt},i}/T_{1/2}^{\text{cal},i})]^2/178}$. These results illustrate that the potential depth V_N, when expressed as a function of fundamental physical quantities—such as mass number A, charge number Z, shell correction

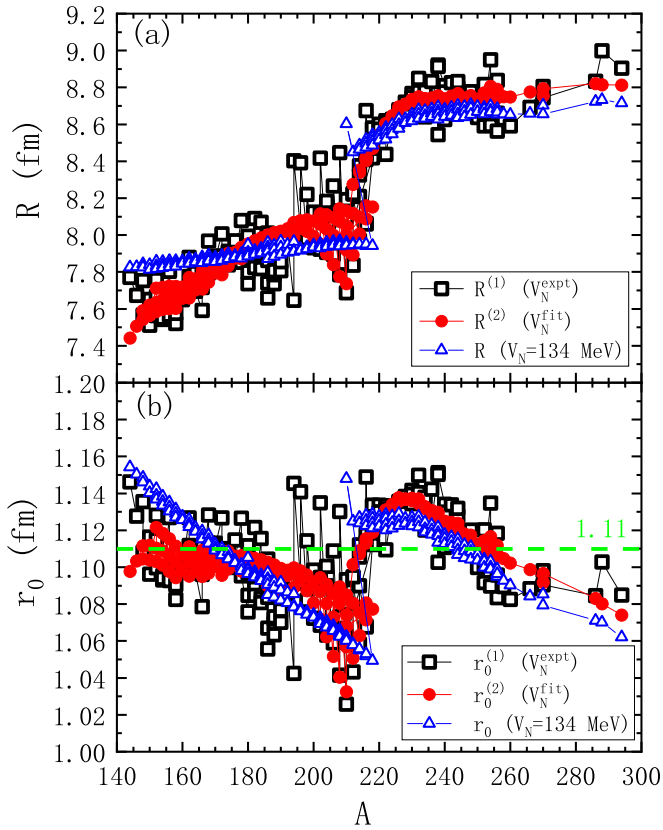

FIG. 3. Comparison of the calculated values of R with three different potential depths: (a) the extracted depth $V_N^{\rm expt}$ (open squares), $V_N^{\rm fit}$ (solid circles), and $V_N = 134$ MeV (open triangles); (b) the same as in Fig. 3(a) but for the reduced radius $r_0 = R/(A_\alpha^{1/3} + A_d^{1/3})$.

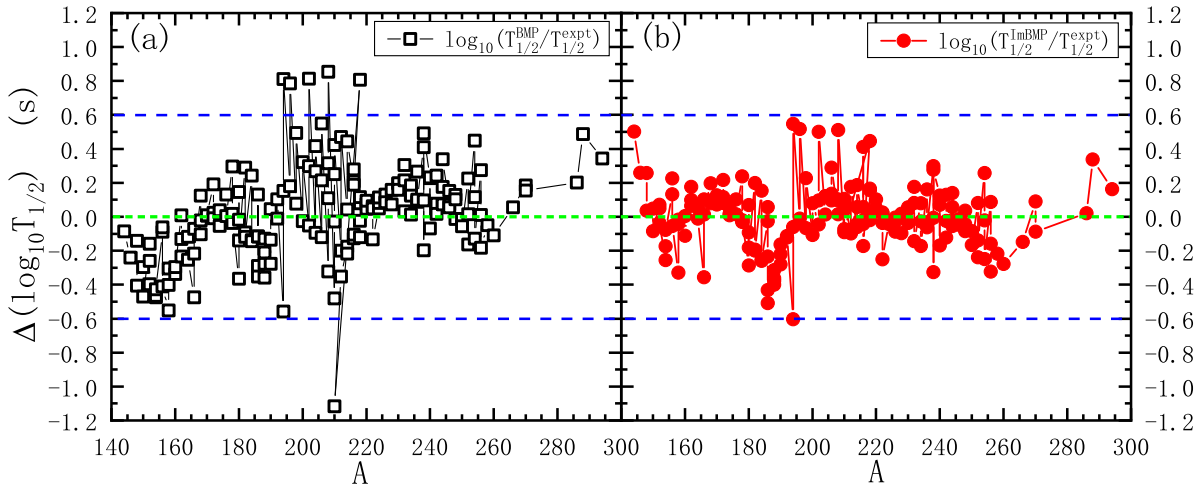

FIG. 4. Comparison of the logarithmic deviation of half-lives calculated by the BMP model (a), and by the improved BMP model using $V_N^{\rm fit}$ (b) versus the mass numbers of α emitters.

energy $E_{\rm sh}$, and Q value—can effectively capture structural effects within parent nuclei.

III. THE RESULTS AND DISCUSSIONS

The square-well radius R is another key physical quantity in our analysis. Buck, Merchant, and Perez [16,17] argued that the square-well radius should not be determined from the charge radius. Instead, it should be derived from the Bohr-Sommerfeld condition for an α-particle wave function inside the nucleus, accounting for a fixed potential depth and number of nodes. Using this method, we calculated the radii $R^{(1)}$, $R^{(2)}$, and R from Eq. (3) using three different potential depths of $V_N^{\rm expt}$, $V_N^{\rm fit}$, and $V_N = 134$ MeV. The quantum number G is set to 22 for $N \leqslant 126$ and 24 for $N > 126$. The values $R^{(1)}$ and $R^{(2)}$ are listed in column 6 and column 7 of Table I. The open squares, solid circles and open triangles denote the calculated R values based on the three different potential depths, as shown in Fig. 3(a). As shown in Fig. 3(a), the calculated $R^{(2)}$ values from Eq. (12) align more closely with the experimental $R^{(1)}$ values compared to those calculated with $V_N = 134$ MeV from the BMP model. Thus, the potential radius is also influenced by the potential depth. We also show the behavior of the reduced radius $r_0 = R/(A_\alpha^{1/3} + A_d^{1/3})$ for 178 even-even nuclei as a function of mass number A in Fig. 3(b). Here the spherical square-well radius R is assumed to be equal to the sum of the radii of both decay fragments. Clearly, r_0 is not constant. It decreases with increasing mass number A for both $N < 126$ and $N > 126$, but increases sharply near $N = 126$. The average value of $r_0^{(1)}$ is 1.11 fm, which is lower than the generally accepted value of 1.2 fm. To better visualize the calculated results, Fig. 4 shows the logarithmic deviation of half-lives for 178 even-even nuclei with proton numbers $Z = 60$ to 118 as a function of mass numbers A. In Fig. 4, the open squares represent the logarithmic deviations calculated by the BMP model, while Fig. 4(b) shows the deviations from the ImBMP model using $V_N^{\rm fit}$ from Eq. (12) (solid circles). The region between the two blue dashed lines indicates the deviation between theoretical and experimental α-decay half-lives, which is mostly within a factor of 0.6. When compared with Fig. 4(a), it is evident that the majority of the calculation results have been significantly improved, with the data points clustering around zero in Fig. 4(b). This indicates that the theoretical results obtained by using Eq. (12) better agree with the experimental data. Synthesis of superheavy elements is an important scientific subject in the fields of nuclear physics and chemistry. Figure 5 plots the predicted $\log_{10} T_{1/2}$ values as functions of N_d (the neutron number of the daughter nucleus) for parent nuclei with $Z = 118$ and 120 isotopes. As shown in Fig. 5, the calculated values from the ImBMP model are highly consistent with the predictions from the Deng-Zhang-Royer (DZR) model [33]. Moreover, the result of the ImBMP model is in the best agreement with the experimental data of ^{294}Og (open star). In contrast, the BMP model somewhat overestimates the DZR model's results. In addition, the shell effects at the neutron numbers $N_d = 178$ and 184 are evident for both cases with $Z = 118$ and 120 isotopes. In other words, while the calculated α-decay half-life values are model dependent, the predicted magic numbers remain consistent. It is also noteworthy that the calculated half-life of ^{296}Og is longer than the experimental half-life of ^{294}Og, due to its neutron number N_d being close to 178.

IV. SUMMARY

In summary, the potential depth V_N is extracted from the measured α-decay half-lives using an enumeration method based on the BMP model, utilizing 178 experimental data points from even-even nuclei compiled in the NUBASE2020 database. We found that the shell correction is crucial for accurately describing α-decay half-lives. Incorporating shell correction into the potential depth V_N, we derived a new formula by fitting the extracted "experimental" potential depth $V_N^{\rm expt}$. This new formula relies on the fundamental physical quantities of parent nucleus: shell correction energy, mass number, charge number, and Q value. It significantly reduces the rms deviation between theoretical and experimental half-lives by 32%, indicating the method's reliability in determining α-decay half-lives. The formula is also used to

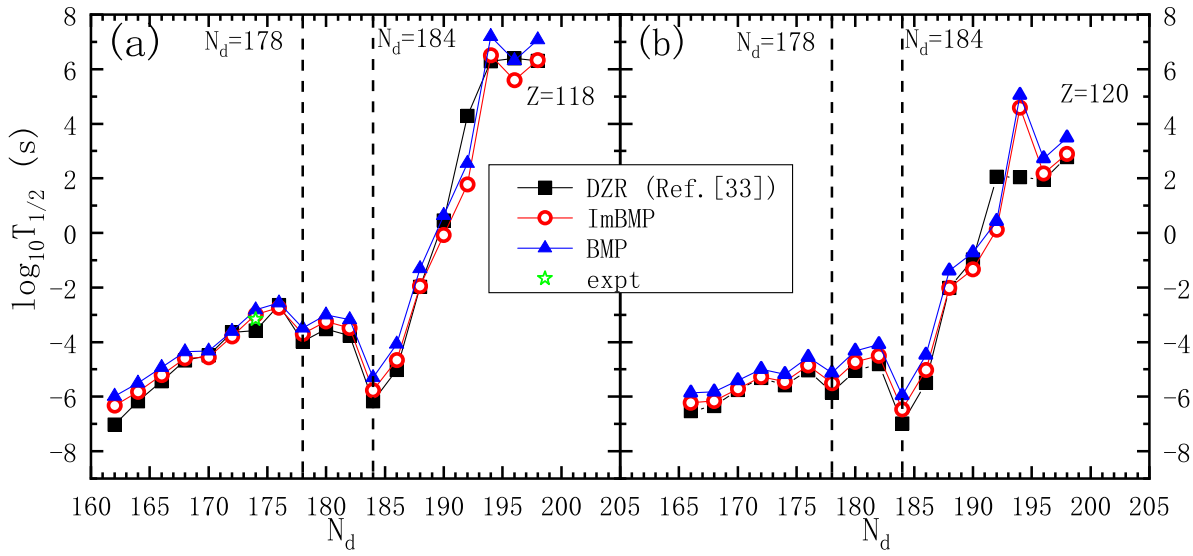

FIG. 5. The $\log_{10} T_{1/2}$ values of $Z = 118$ (a) and 120 (b) isotopes versus neutron number of daughter nucleus N_d. The open circles and the solid triangles denote the prediction results with the ImBMP model and with the BMP model, respectively. Solid squares denote the prediction result of the Deng-Zhang-Royer formula (DZR) by Deng *et al.* [33] for comparison and the open star is the experimental value of ^{294}Og.

predict the α-decay half-lives of superheavy nuclei with $Z = 118$ and 120, and the results agree with those obtained by other methods.

ACKNOWLEDGMENTS

We thank Prof. X. H. Li for helpful communications. This work was supported by the National Natural Science Foundation of China (Grants No. 12465019, No. 12465021, No. 12265006, and No. U1867212), the Guangxi Natural Science Foundation (Grants No. 2023GXNSFDA026005, No. 2023GXNSFBA026008, and No. 2017GXNSFGA198001), and the Central Government Guides Local Scientific and Technological Development Fund Projects (Grant No. Guike ZY22096024).

[1] H. Geiger and J. M. Nuttall, Philos. Mag. **22**, 613 (1911).
[2] G. Gamow, Z. Phys. **51**, 204 (1928).
[3] R. W. Gurney and E. U. Condon, Nature (London) **122**, 439 (1928).
[4] C. Xu and Z. Z. Ren, Nucl. Phys. A **760**, 303 (2005).
[5] C. Xu and Z. Z. Ren, Nucl. Phys. A **753**, 174 (2005).
[6] K. P. Santhosh, B. Priyanka, and M. S. Unnikrishnan, Nucl. Phys. A **889**, 29 (2012).
[7] H. F. Zhang and G. Royer, Phys. Rev. C **77**, 054318 (2008).
[8] V. E. Viola, Jr. and G. T. Seaborg, J. Inorg. Nucl. Chem. **28**, 741 (1966).
[9] C. Qi, F. R. Xu, R. J. Liotta, and R. Wyss, Phys. Rev. Lett. **103**, 072501 (2009).
[10] G. Royer, J. Phys. G: Nucl. Part. Phys. **26**, 1149 (2000).
[11] G. Royer, Nucl. Phys. A **848**, 279 (2010).
[12] D. Ni, Z. Ren, T. Dong, and C. Xu, Phys. Rev. C **78**, 044310 (2008).
[13] D. N. Poenaru, R. A. Gherghescu, and N. Carjan, Europhys. Lett. **77**, 62001 (2007).
[14] Y. Z. Wang, S. J. Wang, Z. Y. Hou, and J. Z. Gu, Phys. Rev. C **92**, 064301 (2015).
[15] K. P. Santhosh, I. Sukumaran, and B. Priyanka, Nucl. Phys. A **935**, 28 (2015).
[16] B. Buck, A. C. Merchant, and S. M. Perez, Phys. Rev. Lett. **65**, 2975 (1990).
[17] B. Buck, A. C. Merchant, and S. M. Perez, J. Phys. G: Nucl. Part. Phys. **17**, 1223 (1991).
[18] A. Bohr and B. R. Mottelson, *Nuclear Structure* (World Scientific, Singapore, 1998).
[19] G. R. Satchler and W. G. Love, Phys. Rep. **55**, 183 (1979).
[20] R. Blendowske and H. Walliser, Phys. Rev. Lett. **61**, 1930 (1988).
[21] J. R. Huizenga and G. Igo, Nucl. Phys. **29**, 462 (1962).
[22] W. J. Dong, Z. Wang, D. Bai, and Z. Z. Ren, Chin. Sci. Bull. **66**, 3581 (2021) (in Chinese).
[23] J. Zhang and H. F. Zhang, Phys. Rev. C **102**, 044308 (2020).
[24] B. Buck, A. C. Merchant, and S. M. Perez, Phys. Rev. C **45**, 2247 (1992).
[25] B. Buck, J. C. Johnston, A. C. Merchant, and S. M. Perez, Phys. Rev. C **52**, 1840 (1995).
[26] M. Wang, W. Huang, F. Kondev, G. Audi, and S. Naimi, Chin. Phys. C **45**, 030003 (2021).
[27] N. Wang, M. Liu, X. Wu, and J. Meng, Phys. Lett. B **734**, 215 (2014).
[28] R. Sharma, A. Jain, P. K. Sharma, S. K. Jain, and G. Saxena, Phys. Scr. **97**, 045307 (2022).
[29] Z. Y. Wang, Z. M. Niu, Q. Liu, and J. Y. Guo, J. Phys. G: Nucl. Part. Phys. **42**, 055112 (2015).

[30] S. A. Gurvitz and G. Kalbermann, Phys. Rev. Lett. **59**, 262 (1987).
[31] O. Bayrak, J. Phys. G: Nucl. Part. Phys. **47**, 025102 (2020).
[32] F. Kondev, M. Wang, W. Huang, S. Naimi, and G. Audi, Chin. Phys. C **45**, 030001 (2021).
[33] J. G. Deng, H. F. Zhang, and G. Royer, Phys. Rev. C **101**, 034307 (2020).

Correction: Typographical errors in Eqs. (4) and (7) have been fixed.